Numerical simulations of transportational cyclic steps

Sergio Fagherazzi[a],*, Tao Sun[b]

[a] *Department of Geological Sciences, School of Computational Science and Information Technology, Florida State University, Dirac Science Library, Tallahassee, FL 32306-4120, USA*
[b] *Department of Geological Sciences and Center for Earth Surface Processes Research, Florida State University, Tallahassee, FL 32306, USA*

Abstract

A numerical model that couples water flow and sediment transport over a non-cohesive bed is developed to simulate the initiation and evolution of transportational cyclic steps. Transportational cyclic steps are periodic bedforms characterized by corresponding hydraulic jumps that form when a supercritical flow erodes and deposits bottom sediments on a steep bed. The flow transition at the hydraulic jump leads to bed erosion on the supercritical part and deposition on the subcritical part of the step, with consequent upstream migration while the form is preserved. The numerical scheme developed to study transportational cyclic steps utilizes an approximate Riemann solver to capture the exact location of the hydraulic jumps present in the domain. Simulations of step growth from small perturbations on an initially flat bed are carried out and partly answer the question of how transportational steps form. Results show that both an initial infinitesimal bottom perturbation and a random distribution of bottom elevations evolve in a series of steps migrating upstream. Moreover, numerical simulations clearly show that the final configuration strongly depends on initial conditions.
© 2003 Elsevier Ltd. All rights reserved.

Keywords: Transportational steps; Hydraulic jump; Supercritical flow; Riemann solvers; Steps and pools

1. Introduction

Uniform water flow over a steep erodible bed creates, in particular conditions, periodic bedforms characterized by corresponding hydraulic jumps. The coupling of water flow and suspended sediment transport produces a spatially varying pattern of deposition and erosion that initiates and subsequently maintains upstream migrating bottom steps. Each step is divided into two parts, with a flat or gently sloping sill where the flow is subcritical and a steep lee side where the flow is supercritical. Two contiguous steps are further connected by a hydraulic jump and the corresponding flow transition leads to increased bed erosion on the supercritical side and increased deposition on the subcritical side, with

consequent step migration. Over a wavelength, deposition balances erosion thus preserving the shape of the steps. This spontaneous formation of bedforms was termed transportational cyclic steps by Whipple et al. (1998), when they observed this peculiar phenomenon in their alluvial fan experiments. Transportational cyclic steps were also noticed in the Netherlands, during the construction of sand dams. When a hyperconcentrated sand–water mixture, guided by two man-made bunds along the sandbody, was flowing from the pipelines toward the head of the dam under construction, a terrace-like sand bed formed on the dam (Winterwerp et al., 1992). This unexpected bed topography raised the engineering concern in how steps affect the efficiency of sediment transport. Based on these observations, Winterwerp et al. (1992) calculated the water flow velocity and sediment concentration using a fixed bed profile with steps.

---

*Corresponding author. Tel.: 850-644-4274; fax: 850-644-0098.

E-mail address: sergio@csit.fsu.edu (S. Fagherazzi).

Flume experiments carried out by Taki and Parker (in press) shed light on the formation and evolution of transportational cyclic steps. In these experiments water and sediment were introduced at a constant rate from the upstream end of a flume, while at the downstream end both were allowed to escape freely across a low tail weir. In the first part of the experiment, the sediment bed prograded and aggradated towards and equilibrium profile. Once this equilibrium profile was reached, steps started forming at the downstream end of the flume and migrated upstream at a constant speed. This allowed to obtain measurements of equilibrium slope and water depth both in absence and presence of steps. Taki and Parker were then able to study the step shape as a function of discharge, sediment concentration and average bottom slope. A recent mathematical model proposed by Sun and Parker (in press) represents a major improvement in our understanding of transportational cyclic steps. The theory is based on the observation that cyclic steps migrate upstream while maintaining a constant shape, and therefore seeks for the self-preserving solution of the governing equations. In transportational steps, erosion and deposition are in equilibrium, so that the average elevation of the bed remains constant during the step formation and migration. Shape and dimension of steps, as well as the upstream migration speed, are predicted by the theoretical model as a function of water discharge and suspended sediment concentration. This nonlinear theory explains the regime of formation of transportational cyclic steps, which depends on the Froude number of the flow in absence of steps and on the threshold condition for bed erosion. The corresponding results compare favorably with experimental data (Taki and Parker, in press), producing steps with dimensions of the same order of magnitude of real steps. Finite-slope effects near the downstream end of the step, inaccuracy in the measurement of water depth, and some model simplifications (the hypothesis of constant sediment concentration in the vertical and the neglecting of bedload sediment transport) however reduce the accuracy of the theoretical results.

Closely related to that of Sun and Parker (in press), a mathematical model for steps that form in absence of sediment deposition (named erosional cyclic steps to differentiate them from transportational cyclic steps) has been developed by Parker and Izumi (2000). In Parker and Izumi's model, it is assumed that once the material is eroded from the bed, it is carried out of the system as washload without redeposition. In the purely erosional picture, the transport of sediment is not considered and the entire system constantly degrades. While erosional cyclic steps often form in cohesive beds, such as in hillslopes with abundant clay or organic materials (Izumi and Parker, 2000), in environments characterized by sand the transport and redeposition of sediment play an important role in the process.

Both Winterwerp et al.'s and Sun and Parker's mathematical models for transportational cyclic steps are based on a steady bottom configuration consisting of a regular series of steps equally spaced. In Winterwerp et al. (1992) the step is supposed to be formed by three consecutive segments: the terrace, the sill, and the lee side. The length of the three segments as well as the water height and sediment concentration are determined solving the equations that govern the water flow and sediment transport. In these equations no temporal derivatives are considered (steady state).

In Sun and Parker (in press) the shape of the step is not set a priori but is calculated as part of the solution. The equations governing the water flow field and the suspended sediment transport are steady, without temporal derivatives. The bottom instead can vary in time, producing the step migration. Both models start from an already existing step in equilibrium with other identical steps, and are therefore unable to capture the transient evolution of the steps and, in particular, their formation.

Herein a numerical model based on the complete set of equations is developed and utilized to study the formation and evolution of transportational steps in time and space. Since hydraulic jumps are in any effect shock waves propagating in the domain, it is possible to utilize methods developed for discontinuous solutions of hyperbolic equations, in the framework of conservation laws (LeVeque, 1992). The system of equations is thus resolved utilizing a first order Riemann solver, which is able to capture the hydraulic jump and the complex interaction between water flow and sediment transport. Even though more accurate techniques are already available for the study of hydraulic jumps, based on second order shock-capturing methods (Burguete and Garcia-Navarro, 2001; LeVeque, 1992), herein a first order scheme is utilized for its simplicity, robustness, and for the absence of spurious oscillations that can poison the final results. The final goal of this work is not the development of a new numerical scheme but the utilization of a widely accepted scheme for the study of a physical process. Furthermore, a detailed discussion of the coupling between the De Saint Venant equations and the sediment transport equations is presented. This discussion is the extension of the theory of shock waves in shallow waters (easily found in Stoker, 1957; LeVeque, 1992) to the new system of equations. The present numerical model is developed to study transportational steps created by a supercritical flow with a small water depth, highly concentrated suspended sediment, and a sand bed with constant granulometry.

A succession of steps and pools with related hydraulic jumps also exists in mountain streams (Chin, 1989; Chartrand and Whiting, 2000). Contrary to transportational cyclic steps observed in experiments or during engineering works, the formation of natural steps and

pools is influenced by several factors, as, for example, the sediment granulometry spanning from silt to boulders, the presence of a bedrock surface, and the intensity and frequency of rainfall discharges. The present paper can thus represent a first step toward a more comprehensive model suitable for studying the formation and evolution of mountain steps and pools in spatially heterogeneous and time-varying geological settings.

2. The equations

Four equations describe the formation and evolution of transportational steps. The water flow is governed by the one-dimensional De Saint Venant equations (continuity and conservation of linear momentum):

$$\frac{\partial h}{\partial t} + \frac{\partial uh}{\partial x} = 0, \tag{1}$$

$$\frac{\partial u}{\partial t} + u\frac{\partial u}{\partial x} = -g\frac{\partial h}{\partial x} - g\frac{\partial \eta}{\partial x} - \frac{C_f}{h}u^2, \tag{2}$$

where x is a downstream coordinate, h is the water depth, t denotes time, u is the depth averaged velocity, η the elevation of the bed above a reference level, g is the gravity acceleration and C_f a friction coefficient. The conservation of suspended sediment in the water column can be written as

$$\frac{\partial h\chi}{\partial t} + \frac{\partial uh\chi}{\partial x} = v_s(E - r\chi) \tag{3}$$

with χ the volume concentration of suspended sediment averaged over the vertical, v_s the settling velocity, E the rate of entrainment of sediment from the bed into suspension, r the ratio between near bed sediment concentration and depth-averaged concentration. Since the considered water depths are small, we suppose that the sediment concentration is uniform along the vertical and we set $r = 1$. Eq. (3) states that the temporal variation of suspended sediment volume in the water column is equal to the divergence of the suspended sediment flux plus (minus) the sediment volume entrained (deposited) at the bottom.

The fourth equation (Exner equation) links the local variation in bed elevation to the sediment removed or accumulated at the bottom. It reads

$$(1 - n)\frac{\partial \eta}{\partial t} = v_s(r\chi - E), \tag{4}$$

where n is the porosity of the bed sediments. To close system (1)–(4) the nondimensional entrainment function E needs to be specified. Several examples of entrainment functions E for cohesionless sediments can be found in Garcia and Parker (1991). Here we use the empirical relationship utilized in Sun and Parker (in press) to model the experiments of Taki and Parker (in press):

$$E = \alpha_t[\tau^* - \tau_{th}^*]^n, \tag{5}$$

where τ_{th}^* is the threshold Shields stress for the entrainment of sediment into suspension, α_t an empirical coefficient, n is an exponent ranging between 1.5 and 2.0, and τ^* a Shields stress given by the relationships

$$\tau^* = \frac{\tau}{(\rho_s - \rho)gD}, \quad \tau = \rho C_f u^2 \tag{6}$$

with τ the bottom shear stress, D sediment grain size, ρ and ρ_s density of water and sediment respectively. As showed in Taki and Parker (in press) the coefficient α_t and the critical Shields stress τ_{th}^* are empirically related to a particle Reynolds number and can be determined as a function of the sediment characteristics. With the aid of (6), the entrainment function is rewritten as

$$E = \begin{cases} \alpha_t(\tau_{th}^*)^n\left[\left(\frac{u}{u_{th}}\right)^2 - 1\right]^n & \text{if } u > u_{th}, \\ 0 & \text{if } u \leqslant u_{th}, \end{cases} \tag{7}$$

where

$$u_{th} = \left[\frac{(\rho_s - \rho)gD\tau_{th}^*}{\rho C_f}\right]^{1/2} \tag{8}$$

is the threshold velocity for sediment entrainment.

System (1)–(4) is hyperbolic and nonlinear, therefore discontinuous solutions might form in the domain when time advances (shock waves). In order to correctly capture these weak solutions, the system of equations is reformulated in conservation form, introducing the following conservative variables:

$$q = hu, \quad \psi = h\chi, \quad m = (1 - n)\eta + h\chi, \tag{9}$$

where q is the discharge, ψ the suspended sediment in the water column, and m the sediment volume in a vertical column above a reference level that can be separated in the sediment volume belonging to the bed $(1 - n)\eta$, and the suspended sediment in the water $h\chi$ (Fig. 1). System
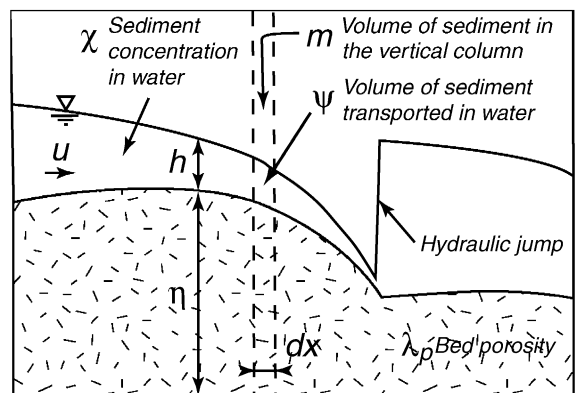

Fig. 1. Notation.

(1)–(4) can thus be rewritten as

$$\frac{\partial \mathbf{U}}{\partial t} + \frac{\partial \mathbf{F}}{\partial x} = \mathbf{S}, \tag{10}$$

where $\mathbf{U}$ is the vector of the conserved variables, $\mathbf{F}$ the flux and $\mathbf{S}$ the source term. They read

$$\mathbf{U} = \begin{bmatrix} h \\ q \\ \psi \\ m \end{bmatrix}, \quad \mathbf{F} = \begin{bmatrix} q \\ q^2/h + \frac{1}{2}gh^2 \\ (\psi q)/h \\ (\psi q)/h \end{bmatrix},$$

$$\mathbf{S} = \begin{bmatrix} 0 \\ -gh(\partial \eta/\partial x) - C_f u^2 \\ v_s(E - r\psi/h) \\ 0 \end{bmatrix}. \tag{11}$$

The source term equal to zero in the first and fourth equations of (10) shows that the total volume of water and the total volume of sediments are conserved in time. On the other hand, linear momentum may vary, increasing or decreasing because of the gravity force on a tilted bottom. At the same time momentum is also reduced by bottom friction. The sediment volume in suspension may change as well, because of deposition or entrainment at the bottom.

3. The Riemann problem

In order to solve system (10), we first study in detail the homogeneous case, governed by the system:

$$\frac{\partial \mathbf{U}}{\partial t} + \frac{\partial \mathbf{F}}{\partial x} = 0. \tag{12}$$

Moreover, we suppose that the initial conditions are the union of two states, a left state (L) and a right state (R), with constant conservative quantities. Since the right values are different from the left values, a discontinuity in $\mathbf{U}$ rises at the contact point (Riemann problem). To solve the Riemann problem, we study the Jacobian of the flux

$$\mathbf{A} = \begin{pmatrix} 0 & 1 & 0 & 0 \\ c^2 - u^2 & 2u & 0 & 0 \\ -u\chi & \chi & u & 0 \\ -u\chi & \chi & u & 0 \end{pmatrix}, \tag{13}$$

where, by definition, $A_{ij} = \partial F_i/\partial U_j$. Its eigenvalues are

$$\lambda_1 = u - c, \quad \lambda_2 = u + c, \quad \lambda_3 = u, \quad \lambda_4 = 0, \tag{14}$$

where $c = \sqrt{gh}$ is the celerity of small amplitude gravitational waves.

The corresponding eigenvectors are

$$\mathbf{r}_1 = \begin{bmatrix} 1 \\ u - c \\ \chi \\ \chi \end{bmatrix}, \quad \mathbf{r}_2 = \begin{bmatrix} 1 \\ u + c \\ \chi \\ \chi \end{bmatrix},$$

$$\mathbf{r}_3 = \begin{bmatrix} 0 \\ 0 \\ 1 \\ 1 \end{bmatrix}, \quad \mathbf{r}_4 = \begin{bmatrix} 0 \\ 0 \\ 0 \\ 1 \end{bmatrix}. \tag{15}$$

Because one eigenvalue is zero the system is degenerate. Each eigenvalue (and corresponding eigenvector) describes a characteristic field, and identifies a family of characteristic lines. On these lines information travels with celerity equal to the associated eigenvalue. According to the theory of hyperbolic equations, the general solution in time of the Riemann problem can be a rarefaction wave, a shock wave or a contact discontinuity for each characteristic field (LeVeque, 1992). In a rarefaction wave the conserved quantities vary continuously, whereas in a shock there is a jump in their value. Finally, a contact discontinuity is a discontinuity that is advected linearly with speed equal to the characteristic speed λ.

From (14) and (15) the following relationships are derived

$$\boldsymbol{\nabla}\lambda_1 \cdot \mathbf{r}_1 \neq 0, \tag{16a}$$

$$\boldsymbol{\nabla}\lambda_2 \cdot \mathbf{r}_2 \neq 0, \tag{16b}$$

$$\boldsymbol{\nabla}\lambda_3 \cdot \mathbf{r}_3 = 0, \tag{16c}$$

$$\boldsymbol{\nabla}\lambda_4 \cdot \mathbf{r}_4 = 0, \tag{16d}$$

showing that the first two characteristic fields are genuinely nonlinear, the third and the fourth are instead linearly degenerate (Lax, 1957). In other words, Eq. (16a), Eq. (16b) are the necessary conditions for the propagation speeds λ_1 and λ_2 to monotonically increase and decrease in a rarefaction wave. Since these two eigenvalues are referred to the De Saint Venant equations, Eq. (16a), Eq. (16b) show that a rarefaction wave is a possible solution for these characteristic fields. As a consequence, the solution of the Riemann problem for the De Saint Venant equations consists of two shocks, two rarefaction waves or a shock plus a rarefaction wave.

On the contrary, Eqs. (16c), (16d) state that in the third (λ_3) and fourth (λ_4) characteristic fields we can have neither rarefaction waves nor shocks, and therefore the solution of the Riemann problem is a contact discontinuity. This can also be seen for the sediment concentration combining the first and third equations

of Eq. (12):

$$\frac{\partial \chi}{\partial t} + u \frac{\partial \chi}{\partial x} = 0. \tag{17}$$

An initial discontinuity in concentration χ travels undisturbed in the flow field with celerity u, without mixing of sediment particles through the discontinuity (we note that system Eq. (12) is based on the assumption of negligeble molecular and turbulent viscosity and related mixing).

Where there is a jump in the variables, the left (L) and right (R) states of a Riemann problem are linked through the Rankine–Hugoniot conditions, written as

$$s = \frac{\mathbf{F}(\mathbf{U}_R) - \mathbf{F}(\mathbf{U}_L)}{\mathbf{U}_R - \mathbf{U}_L}, \tag{18}$$

where s is the speed of the shock or contact discontinuity. For system Eq. (11), the Rankine–Hugoniot conditions are then

$$h_R u_R - h_L u_L = s(h_R - h_L),$$

$$\left(u_R^2 h_R + \frac{1}{2} g h_R^2 \right) - \left(u_L^2 h_L + \frac{1}{2} g h_L^2 \right) = s(h_R u_R - h_L u_L),$$

$$\chi_R u_R h_R - \chi_L u_L h_L = s(\chi_R h_R - \chi_L h_L),$$

$$\chi_R u_R h_R - \chi_L u_L h_L = s[(1-n)\eta_R + \chi_R h_R \\ - (1-n)\eta_L - \chi_L h_L]. \tag{19}$$

When there is a discontinuity in water depth and velocity, the first two equations of (19) represent the standard hydraulic jump conditions (Henderson, 1966).

From the third and fourth Rankine–Hugoniot conditions we can derive the relationship:

$$\eta_R - \eta_L = 0. \tag{20}$$

The bottom elevation is then continuous both at the shock and contact discontinuity locations. For the contact discontinuity, defined by the condition of no mass flow through the discontinuity ($u_L = u_R$), and continuous water depth ($h_L = h_R$), we note that Eq. (19) are satisfied irrespective of the values of χ_L and χ_R. For a shock with $u_L \neq u_R$ and $h_L \neq h_R$, it is possible to derive from the first and third Rankine–Hugoniot conditions:

$$(\chi_R - \chi_L)(u_R - u_L) = 0. \tag{21}$$

This equation is satisfied only if the concentration is continuous at the shock location.

4. The numerical method

We solve system Eq. (10) on a regular Cartesian grid with a finite difference scheme. At the generic point i of the grid, system Eq. (10) can be descritized with the following first order upwind scheme:

$$\dot{\mathbf{U}}_i + \frac{1}{\Delta x}[\mathbf{F}_{i+1/2} - \mathbf{F}_{i-1/2}] = \mathbf{S}_i, \tag{22}$$

where $\dot{\mathbf{U}}_i$ is the temporal derivative of the conserved variables at the point i, Δx is the distance between two mesh points, and $\mathbf{F}_{i+1/2}(\mathbf{U}_{i-1}, \mathbf{U}_i)$, $\mathbf{F}_{i-1/2}(\mathbf{U}_i, \mathbf{U}_{i+1})$ are suitable flux functions that connect the states $\mathbf{U}_{i-1}, \mathbf{U}_i$ and $\mathbf{U}_i, \mathbf{U}_{i+1}$ resolving the corresponding local Riemann problems. Here we utilize the numerical flux based on the Roe's approximate Riemann solver. The corresponding flux function will be studied in detail in the following paragraph. Since the source term $\mathbf{S}$ becomes stiff (i.e. it grows consistently) when the bottom slope is high, a fully explicit scheme in time for Eq. (22) must not only satisfy the Courant–Friedrichs–Lewy condition for the advection term, but it also has to resolve the relaxation time connected to the source term (Jin, 1995). For a stiff source term, solving the relaxation time implies the utilization of a very small time step, thus limiting the applicability of the method.

To circumvent the problem, the source term is treated implicitly, using a simple predictor–corrector scheme. The predictor step is

$$\mathbf{U}_i^{n+1/2} = \mathbf{U}_i^n - \frac{\Delta t}{2\Delta x}[\mathbf{F}_{i+1/2}^n - \mathbf{F}_{i-1/2}^n] + \mathbf{S}_i^n \tag{23}$$

with U_i^n the solution at time n and Δt the time step. Whereas the corrector step is

$$\mathbf{U}_i^{n+1} = \mathbf{U}_i^n - \frac{\Delta t}{\Delta x}[\mathbf{F}_{i+1/2}^{n+1/2} - \mathbf{F}_{i-1/2}^{n+1/2}] + \mathbf{S}_i^{n+1}. \tag{24}$$

The implicit corrector step is then resolved with functional iteration until convergence, i.e. correcting iteratively the value of U_i^{n+1}. The method is first order in time, avoiding in this way a oscillatory behavior if the relaxation time is unresolved (Lowrie and Morel, 2000). The source term is calculated at the point i, and the only space derivative present in it, the slope gradient, is descritized with a centered difference scheme.

5. The Roe numerical flux

The determination of the numerical flux hinges on the solution of a Riemann problem at the boundary of two elements (see Toro, 1992). Following Roe (1981), instead of solving the original nonlinear system derived from the Riemann problem, a modified conservation law is solved, leading to a linear system:

$$\frac{\partial \hat{\mathbf{U}}}{\partial t} + \hat{\mathbf{A}}(\mathbf{U}_L, \mathbf{U}_R) \frac{\partial \hat{\mathbf{U}}}{\partial x} = 0. \tag{25}$$

The matrix $\hat{\mathbf{A}}$, with constant coefficients, depends on the states at the left and at the right of the boundary, and has to respect particular conditions (Roe, 1981). A way to derive the matrix is to calculate the Jacobian of the flux for some average values of $\mathbf{U}$, i.e. $\hat{\mathbf{A}} = \mathbf{A}(\mathbf{U}_{ave})$. For the shallow water equations, the averages can be defined

as (Alcrudo and Garcia-Navarro, 1993; Glaister, 1993)

$$\bar{u} = \frac{c_L u_L + c_R u_R}{c_L + c_R}, \quad \bar{c} = \sqrt{\frac{1}{2}(c_L^2 + c_R^2)},$$

$$\bar{h} = \frac{1}{2}(h_L + h_R). \tag{26}$$

For the sediment concentration, following the outlines reported in LeVeque (1992), it is possible to show that the average is

$$\bar{\chi} = \frac{c_L \chi_L + c_R \chi_R}{c_L + c_R}. \tag{27}$$

The Roe flux is then

$$\mathbf{F}(\mathbf{U}_L, \mathbf{U}_R) = \frac{1}{2}(\mathbf{F}(\mathbf{U}_L) + \mathbf{F}(\mathbf{U}_L)) - |\hat{\mathbf{A}}|(\mathbf{U}_R - \mathbf{U}_L)$$

$$= \frac{1}{2}(\mathbf{F}(\mathbf{U}_L) + \mathbf{F}(\mathbf{U}_R)) - \sum_i |\bar{\lambda}_i|_{\mathrm{mod}} \Delta w_i \mathbf{r}_i \tag{28}$$

where Δw_i are the wave strengths:

$$\Delta w_1 = \frac{1}{2}(h_R - h_L) + \frac{\bar{h}}{2\bar{c}}(u_R - u_L),$$

$$\Delta w_2 = \frac{1}{2}(h_R - h_L) - \frac{\bar{h}}{2\bar{c}}(u_R - u_L),$$

$$\Delta w_3 = \bar{h}(\chi_R - \chi_L), \tag{29}$$

and the eigenvectors $\mathbf{r}_i$ are calculated with the averaged quantities. The eigenvalues $|\bar{\lambda}_i|_{\mathrm{mod}}$ are equal to

$$|\bar{\lambda}_i|_{\mathrm{mod}} = \begin{cases} |\bar{\lambda}_i| & \text{if } |\bar{\lambda}_i| \geqslant \varepsilon \\ \varepsilon & \text{if } |\bar{\lambda}_i| < \varepsilon \end{cases} \tag{30}$$

to avoid entropy violating shock solutions (see Harten and Hyman, 1983). $|\bar{\lambda}_i|$ are calculated from (14) with the averaged quantities (26), (27) while ε is

$$\varepsilon = \max[0, (\bar{\lambda}_i - \lambda_{Li}), (\lambda_{Ri} - \bar{\lambda}_i)]. \tag{31}$$

In this framework the numerical fluxes in Eq. (23) and Eq. (24) simply become $\mathbf{F}_{i+1/2} = \mathbf{F}(\mathbf{U}_i, \mathbf{U}_{i+1})$, $\mathbf{F}_{i-1/2} = \mathbf{F}(\mathbf{U}_{i-1}, \mathbf{U}_i)$.

6. Threshold bed slope and boundary conditions

A limit solution for the first and second Rankine–Hugoniot equations Eq. (19), subject to the condition $u_L h_L = u_R h_R = q$, is the following:

$$u_L \to \infty, \quad h_L \to 0, \quad u_R \to 0, \quad h_L \to \infty. \tag{32}$$

From a mathematical point of view, given a constant discharge, the velocity can grow indefinitely before the jump, reducing the water depth to zero. As a consequence, after the jump the velocity decreases to zero and the water depth becomes infinite. When this limit solution is coupled with sediment transport, nothing seems to prevent the bottom slope before the jump to grow indefinitely producing increasingly higher velocities. A closure condition is then needed to limit the maximum velocity and stop the deepening of the step. In Sun and Parker (in press) the velocity after the jump is posed equal to the critical velocity for sediment entrainment; herein we instead prefer to limit the maximum slope of the bottom, which is a natural condition for cohesionless sediments. In order to do that, we introduce a multiplicative coefficient for the entrainment function:

$$E' = pE, \quad \text{with}$$

$$p = \begin{cases} 1 & \text{if } \dfrac{\partial \eta}{\partial x} < 0.9 S_{\mathrm{cr}}, \\ \dfrac{\partial \eta / \partial x - 0.9 S_{\mathrm{cr}}}{S_{\mathrm{cr}} - \partial \eta / \partial x} + 1 & \text{if } \dfrac{\partial \eta}{\partial x} \geqslant 0.9 S_{\mathrm{cr}}, \end{cases} \tag{33}$$

where E' is the new entrainment function, S_{cr} the maximum slope for the bed material, and 0.9 an arbitrary number close to 1. Numerical simulations show that the results are not sensitive to the value of this parameter. This is a first approximation, considering that system Eq. (10) has been derived with the assumption of small bottom slope. A more rigorous formulation should consider a finite value of bottom slope for the water flow and sediment transport (Parker and Izumi, 2000). The introduction of the parameter p in the equations leads to a rapid increase in sediment entrainment at the bottom when the slope approaches the maximum value, with a rise of suspended sediment concentration. As a result the slope at the end of each step cannot exceed this value. It is intuitive to suppose that the maximum slope is linked to the angle of repose of the cohesionless sediment forming the bed. As a matter of fact experimental results showed that the maximum slope is less than the angle of repose (Taki and Parker, in press), indicating that the sediment immerse in flowing water is less stable than sediment at repose. We then suppose that the maximum slope can be obtained from experiments.

In order to solve system Eq. (10) suitable boundary conditions have to be imposed. In this paper we implement cyclic boundary conditions, setting the values of discharge, water depth and sediment discharge at the end point $x = L$ equal to the values at the starting point $x = 0$. The bottom slope at the first and last point is written as an average between two backward differences, avoiding in that way to explicitly account for the total difference in bed elevation between the first and the last point, and leaving the bottom slope free to change. In reality, since cyclic boundary conditions are equivalent to an infinite series of domains of length L and slope S, a change in bottom slope becomes impossible during the simulation, because it would create a bottom discontinuity between a domain and the following one.

Finally, with cyclic boundary conditions, the amount of water and the volume of sediment in the domain are conserved during the simulation. To facilitate the

comprehension of the model implementation, a flow chart with all the numerical components is reported in Fig. 2.

7. Numerical simulations

The formation and evolution of transportational cyclic steps is simulated in a domain of length 3 m with a mesh of 150 nodes (a further increase of nodes does
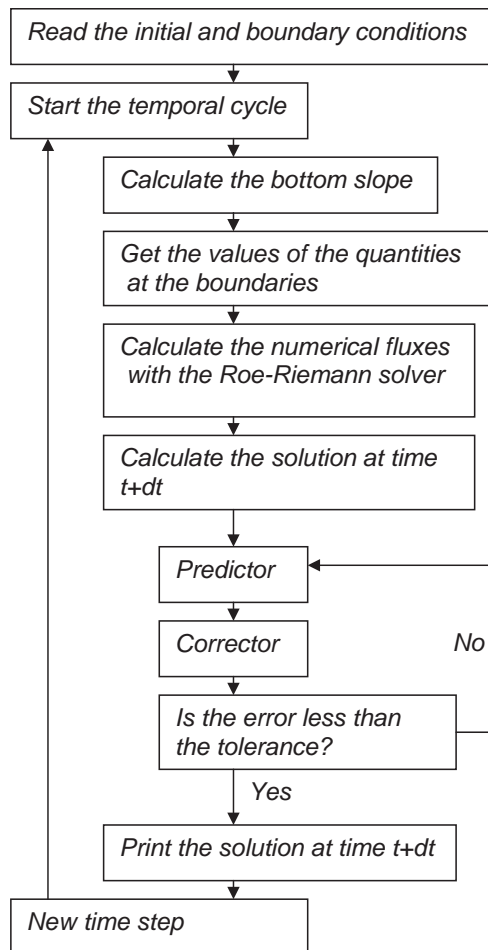

Fig. 2. Flow chart with numerical components of model.

not sensibly change the final result). As showed in Taki and Parker (in press) experiments and supported by the theory of Sun and Parker (in press), the sediment bed evolves toward a stable configuration consisting of a series of hydraulic jumps that creates regular steps at the bottom. The set of parameters utilized in the first simulation is shown in Table 1, and corresponds to the properties of uniform quartz sand having diameter equal to 19 mμ (Taki and Parker, in press). Furthermore, we assume the maximum slope to be equal to 0.46, which is the average value of the experimental results (Taki and Parker, in press).

For the first numerical experiment we start from a uniform flow over a bed of constant slope $S = 0.05$. The flow and the bed are in equilibrium, in the sense that the amount of deposited sediment is equal to the amount of entrained sediment. The initial conditions are then identical to the initial conditions of Taki and Parker's experiments, with a uniform flow over a flat bed. This state is fully identified by setting the source term of the system equal to zero:

$$u_0 = \sqrt{C_f g h_0}, \quad E_0 = \chi_0. \tag{34}$$

Substituting Eq. (7) in Eq. (34) we obtain two equations in four unknowns u_0, h_0, χ_0, S_0. If we specify the slope, another parameter is needed to determine the uniform state. We take a initial discharge $q_0 = h_0 u_0 = 0.002$ m^3/s. The slope is higher than the critical slope hence the flow is in supercritical condition.

In Taki and Parker's experiments the flume end is the location where a perturbation is likely to develop in a hydraulic jump. In the numerical model we can introduce a perturbation (i.e. a bump at the bottom) in any position of the domain and let the system evolve (Fig. 3a). In a first stage the bump is growing until a hydraulic jump forms upstream of the bump since the flow is obliged to become subcritical in order to gain enough specific energy to pass the bump (Fig. 3b). After the top of the bump where, neglecting curvature effects, the critical condition establishes, the flow is accelerated by a slope higher than the initial slope, and it reconnects to the uniform flow with a gradually varying profile. Here the higher velocity produces erosion. On the other hand, just before the bump, the subcritical regime encourages sediment deposition, since the flow velocity

Table 1
Simulation parameters

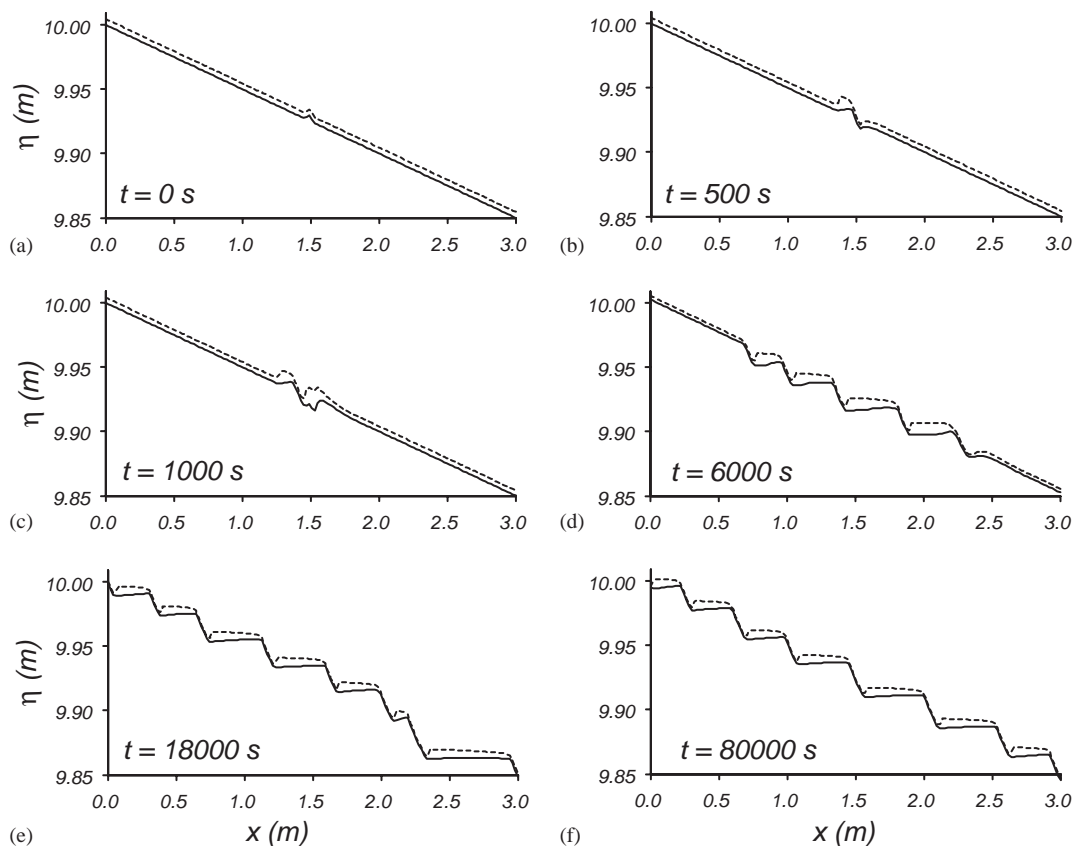| Sediment	D (mμ)	v_s (cm/s)	C_f	u_{th}	τ_{th}^*	α_t ($n = 2$)	S_{cr}
Quartz 19	19	0.032	0.0117	10.13	0.389	0.00169	0.46
Silica 45	45	0.180	0.0134	8.23	0.125	0.0130	0.46
Silica 120	120	1.010	0.0160	10.59	0.092	0.0104	0.46

After Taki and Parker (in press).

Fig. 3. (a)–(f) Formation and evolution of transportational steps from a single bump at bottom. (——-) Bottom; (- - -) water surface.

decreases consistently. Because of this twofold effect the bump migrates upstream. The flow acceleration after the bump significantly scours the bed sediment, lowering the bottom level at an elevation less than the initial elevation. The current thus has to pass an increasingly higher difference in bottom elevation to reconnect to the uniform flow, until this difference is so marked that the flow passes in subcritical condition to gain enough energy (Fig. 3c). A second step thus forms downstream and so on, resulting in the creation of a series of steps. As a final result a perturbation of the initial bottom profile propagates in both directions, with migration of steps upstream and creation of new steps downstream (Fig. 3d). Since we imposed cyclic boundary conditions, the steps migrating upstream will encounter the steps forming downstream, and, after a transition period (Fig. 3e), a steady configuration of identical migrating steps will take place (Fig. 3f).

While the total volume of water and the total amount of sediments in the domain are conserved during the simulation, discharge and suspended sediments decrease from the configuration without steps to the configura-tion with steps. At time $t = 1000$ s the velocity is high and, consequently, the difference in water depth at the hydraulic jump (Fig. 4a–c). On the other hand, at time $t = 80\,000$ s when the steps are steadily migrating upstream, the average velocity is sensibly reduced, as well as the difference in water depth at the hydraulic jump (Fig. 4f, g). The concentration increases where the flow accelerates reducing its depth, while it decreases where the flow is in subcritical conditions (Fig. 4d). We note that the velocity and the water depth have a discontinuity at the hydraulic jump, whereas the concentration is continuous (even though with a steep gradient), as expected from the discussion previously presented.

A second simulation is performed with a tilted bottom to which are added small random elevations selected from a uniform distribution between ± 0.0005 m (Fig. 5a). During the simulation, the initial bottom perturba-tions get amplified until a series of hydraulic jumps forms (Fig. 5b, c). The hydraulic jumps are unevenly distributed at the bottom, depending on the initial conditions. Moreover, because of the high frequency of
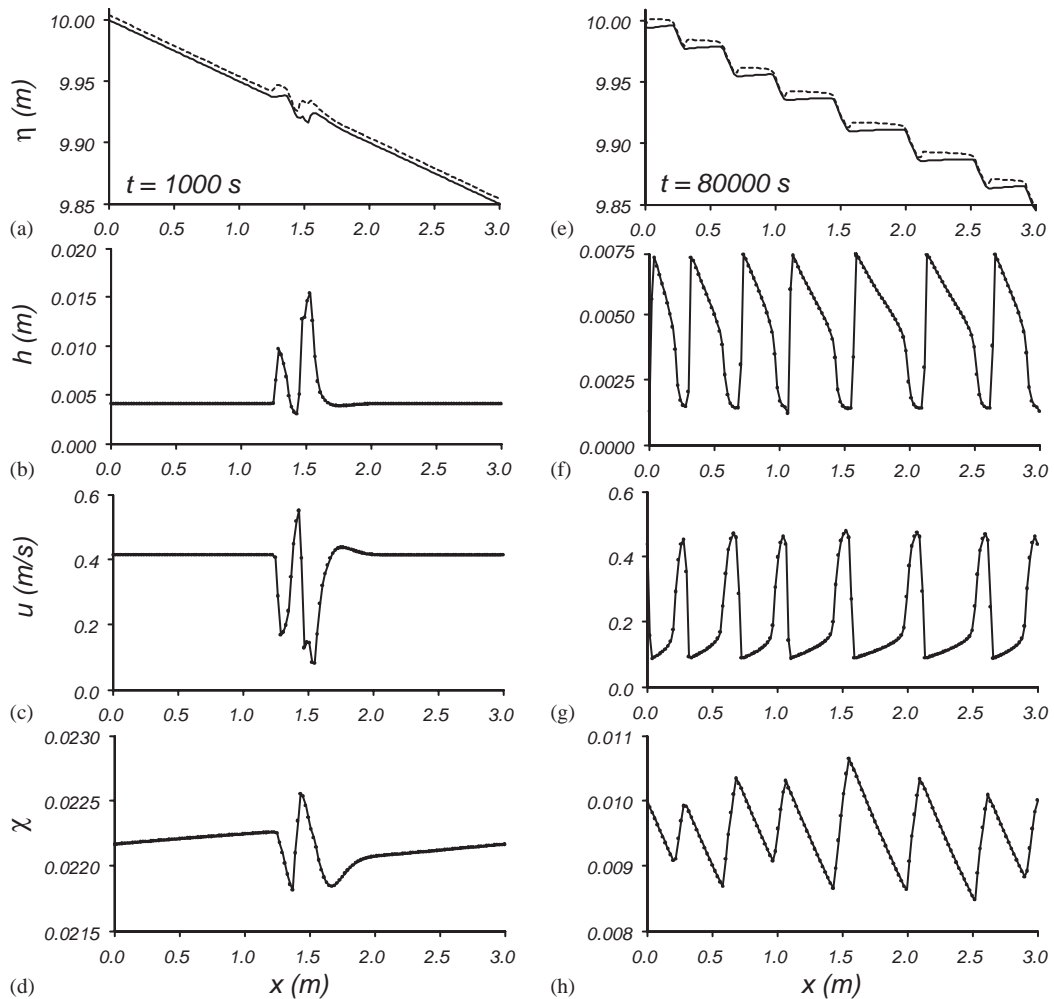
Fig. 4. Comparison between solution at $t = 2000$ s and at $t = 80\,000$ s (steady solution) for simulation showed in Fig. 2. At $t = 2000$ s: (a) bottom and water surface; (b) water depth; (c) velocity; (d) concentration. At $t = 80\,000$ s; (e) bottom and water surface; (f) water depth; (g) velocity; (h) concentration.

the initial perturbation, there are more hydraulic jumps than in the previous simulation. Once formed, the steps migrate upstream at a different speed, trying to reach an equilibrium configuration. To this end, the big jumps compress the small ones until their disappearance, thus reducing the total number of steps (Fig. 5c–e). At the final state, the number of steps is different from the steps formed from a single bottom perturbation (compare Fig. 4 with Fig. 6). This second example clearly shows that initial conditions are of fundamental importance in setting the final number of steps.

Several simulations were performed with different bump elevations. The bump always grew, even for vanishing initial elevation, until a hydraulic jump formed. We further compared the numerical simulations with the experimental results of Taki and Parker (in

press, see Table 5) for three different kinds of sand, whose characteristics are reported in Table 1. The comparison proceeds as follow. As initial conditions we utilize a single bump (see Fig. 3) that corresponds to the experimental conditions (in the experiments a single bump migrates upslope triggering the formation of other bumps). We then fix the slope in the simulation equal to the resulting experimental slope with steps. We try different values for the initial discharge until the final discharge with steps differs less than 10% from the experimental value. The sediment concentration and the step dimensions depend on this initial choice of slope and discharge. The dimensions of the simulated steps have the same order of magnitude of the experimental results (Table 2), but some differences are present in both step length and sediment concentration
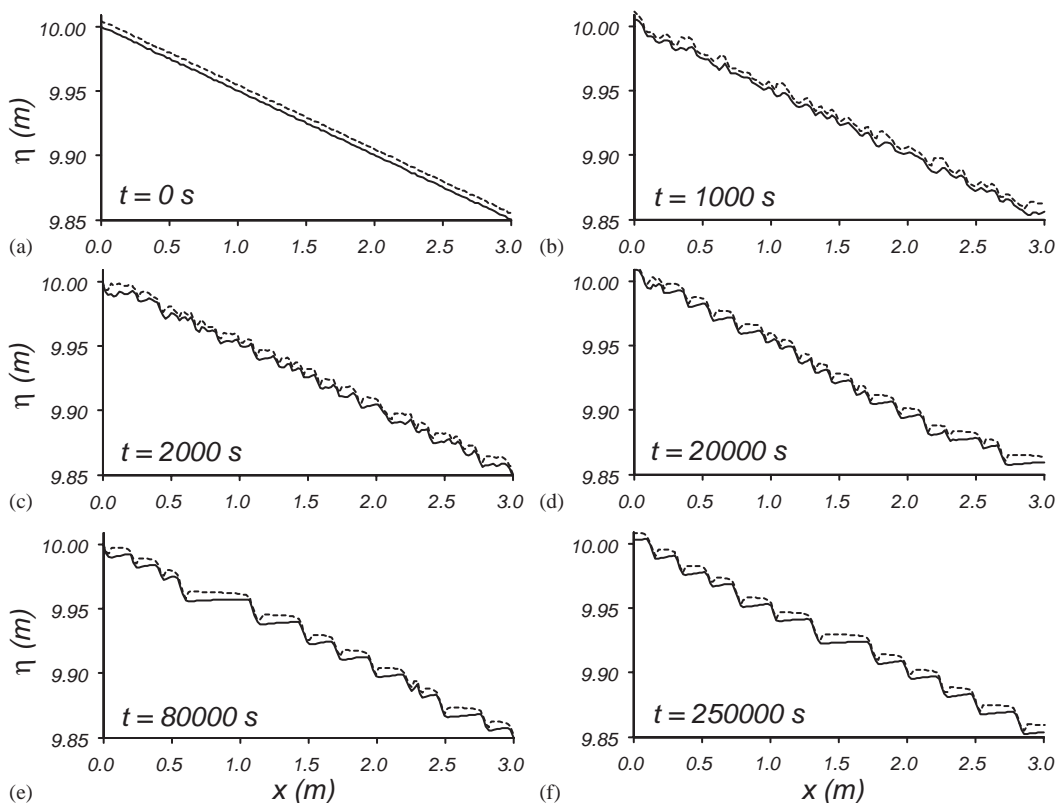
Fig. 5. (a)–(f) Formation and evolution of transportational steps from a bottom with added random perturbation. (——-) Bottom; (- - -) water surface.

(see Table 2). These incongruities reflect the degree of approximation of the sediment parameters reported in Table 1 (see Taki and Parker, in press for a discussion), as well as the sensitivity of the numerical results with respect to the closure hypothesis regarding the bottom maximum slope and the initial conditions. Improvements in both experiments and numerical models are demanded in order to reduce the gap between the results. From a numerical point of view a correct implementation of the full equations keeping in account a finite bottom slope and a deeper investigation regarding the limiting conditions for step growth might consistently improve the model. Comparison of the experimental step shape reported in Taki and Parker (in press, Fig. 8) with a numerical simulation shows that the model is able to capture the structure of the step and related water depth (Fig. 7). Despite the level of approximation involved, we can conclude that the results presented herein are consistent, to a first approximation, with the experiments. It is important to note that the extension of the present model in two- and three-dimensions can provide insights on the planimetric structure of transportational steps and their three-dimensional formation and evolution.

Table 2
Comparison between experiments and simulations

	q (cm^2/s)	χ	S	$\Delta\eta$ (cm)	L (cm)
Quartz 19 run 23	7.14	0.0421	0.0505	2.31	48
Simulation	6.52	0.010	0.0505	2.53	50
Silica 45 run 6	7.00	0.0836	0.0617	2.21	70
Simulation	7.48	0.072	0.0617	2.3	38
Silica 45 run 8	11.08	0.026	0.043	2.77	113
Simulation	11.4	0.074	0.043	2.1	50
Silica 45 run 7	11.06	0.0266	0.0485	2.36	106
Simulation	11.3	0.091	0.0485	2.4	50
Silica 120 run 7	11.9	0.030	0.0655	2.55	49
Simulation	11.6	0.014	0.0655	1.83	28
Silica 120 run 9	14.3	0.0342	0.0723	3.48	65
Simulation	14.0	0.023	0.0723	2.7	38

8. Conclusions

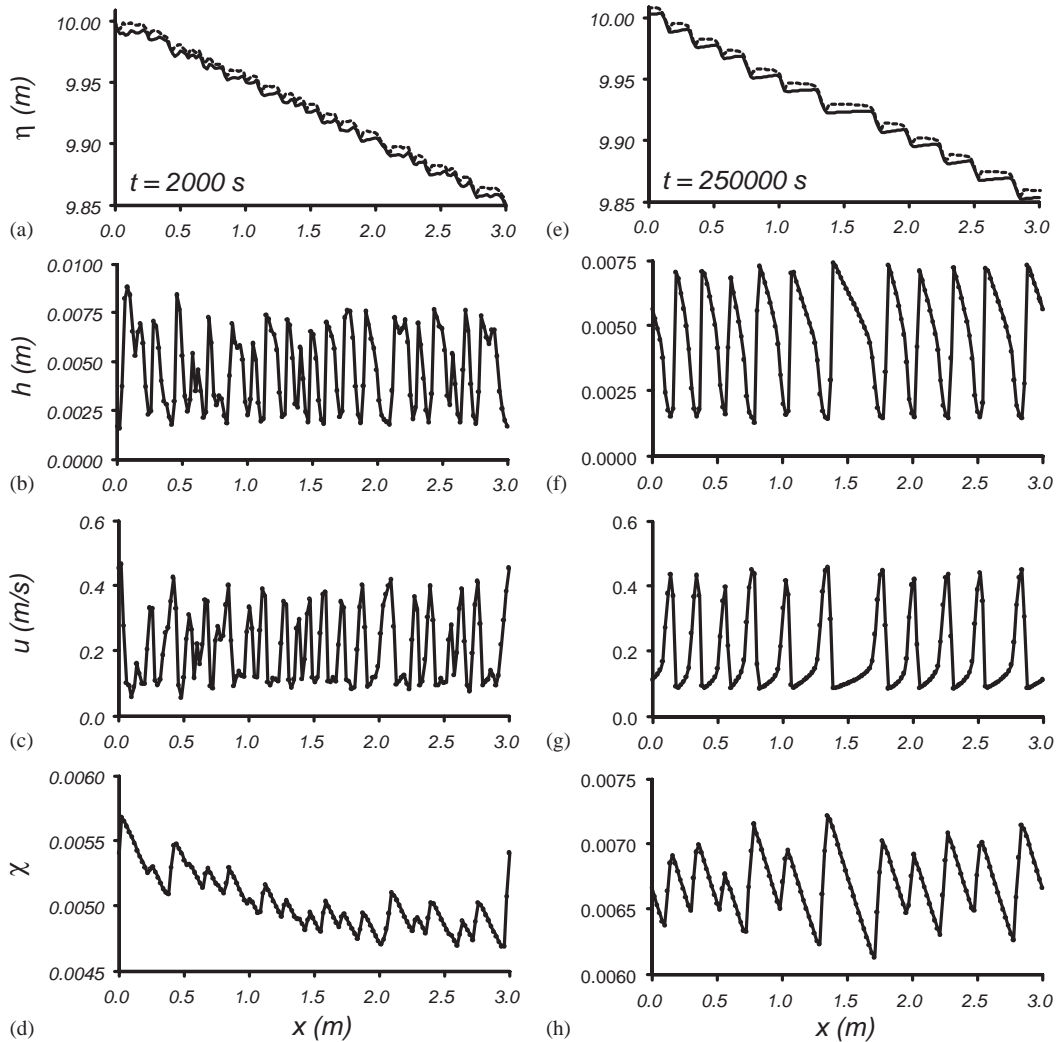A numerical model for the initiation and growth of transportational cyclic steps is presented. An

Fig. 6. Comparison between solution at $t = 2000$ s and at $t = 250\,000$ s (steady solution) for simulation showed in Fig. 4. At $t = 2000$ s: (a) bottom and water surface; (b) water depth; (c) velocity; (d) concentration. At $t = 250\,000$ s; (e) bottom and water surface; (f) water depth; (g) velocity; (h) concentration.
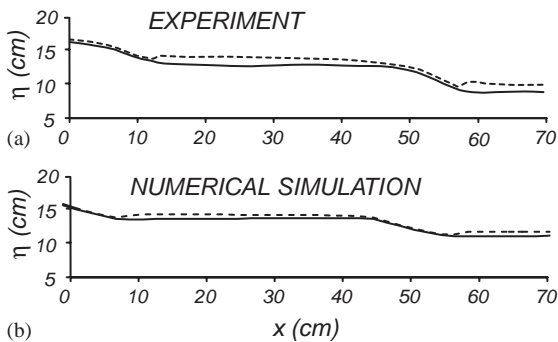

Fig. 7. Comparison between (a) experimental results (from Taki and Parker (in press, fig. 8, Quartz 19 run 24, $q = 7.2$ cm^2/s, $\chi = 0.0448$) and (b) numerical simulation with same parameters. (- - -) Water surface; (——) sediment bottom.

approximate Riemann solver is used to treat the velocity and water depth discontinuities associated with the hydraulic jumps. Results show that an initial infinitesimal bottom perturbation grows in a step with a transition of flow from subcritical to supercritical before and after it. Once formed, the step migrates upstream and triggers the development of new steps in the downstream direction. A series of steps thus appears having same shape and dimensions. On the other hand, a different initial condition, for example a random distribution of bottom elevation, may create a high number of hydraulic jumps. These jumps are not in equilibrium, since they are caused by the high frequency of the initial perturbations. As a result, the bottom is reworked mostly by the bigger jumps that compress the small ones until they are eliminated. Under these

conditions the final number of steps is higher than the steps created by a single perturbation, showing that the equilibrium configuration strongly depends on initial conditions. Comparisons with experiments proves that the simulated steps are consistent, in first approximation, with the real ones.

Acknowledgements

References

Alcrudo, F., Garcia-Navarro, P., 1993. A high-resolution Godunov-type scheme in finite volumes for the 2D shallow-water equations. International Journal for Numerical Methods in Fluids 16 (6), 489–505.

Burguete, J., Garcia-Navarro, P., 2001. Efficient construction of high-resolution TVD conservative schemes for equations with source terms: application to shallow water flows. International Journal for Numerical Methods in Fluids 37 (2), 209–248.

Chartrand, S.M., Whiting, P.J., 2000. Alluvial architecture in headwater streams with special emphasis on step-pool topography. Earth Surface Processes and Landforms 25 (6), 583–600.

Chin, A., 1989. Step pools in stream channels. Progress in Physical Geography 13, 391–407.

Garcia, M., Parker, G., 1991. Entrainment of bed sediment into suspension. Journal of Hydraulic Engineering, American Society of Civil Engineers 117 (4), 414–435.

Glaister, P., 1993. An efficient numerical scheme for the shallow-water equations. International Journal of Computer Mathematics 48 (3–4), 239–250.

Harten, A., Hyman, J.M., 1983. Self-adjusting grid for one-dimensional hyperbolic conservation laws. Journal of Computational Physics 50 (2), 235–269.

Henderson, F.M., 1966. Open Channel Flow. MacMillan, New York, 522pp.

Izumi, N., Parker, G., 2000. Linear stability analysis of channel inception: downstream-driven theory. Journal of Fluid Mechanics 419, 239–262.

Jin, S., 1995. Runge-Kutta methods for hyperbolic conservation-laws with stiff relaxation terms. Journal of Computational Physics 122 (1), 51–67.

Lax, P.D., 1957. Hyperbolic systems of conservation laws 2. Communication on Pure and Applied Mathematics 10 (4), 537–566.

LeVeque, R.J., 1992. Numerical Methods for Conservation Laws. Birkhauser, Berlin, 232pp.

Lowrie, R.B., Morel, J.E., 2000. Discontinuous Galerkin for hyperbolic systems with stiff relaxation. In: Cockburn, B., Karniadakis, G., Shu, C.W., Griebel, M. (Eds.), Discontinuous Galerkin Methods: Theory, Computation and Applications. Lecture Notes in Computational Science and Engineering. Springer, New York, pp. 385–391.

Parker, G., Izumi, N., 2000. Purely erosional cyclic and solitary steps created by flow over a cohesive bed. Journal of Fluid Mechanics 419, 203–238.

Roe, P.L., 1981. Approximate Riemann solvers, parameter vectors, and difference-schemes. Journal of Computational Physics 43 (2), 357–372.

Stoker, J.J., 1957. Water Waves; The Mathematical Theory with Applications. Interscience, New York, 567pp.

Sun, T., Parker, G., Transportational cyclic steps created by flow over an erodible bed. Part 2. Theory and numerical simulation, Journal of Hydraulic Research, in press.

Taki, K., Parker, G., Transportational cyclic steps created by flow over an erodible bed. Part 1. Experiments, Journal of Hydraulic Research, in press.

Toro, E.F., 1992. Riemann problems and the WAF method for solving the 2-dimensional shallow-water equations. Philosophical Transactions of the Royal Society of London Series A-Mathematical Physical and Engineering Sciences 338 (1649), 43–68.

Whipple, K.X., Parker, G., Paola, C., Mohrig, D., 1998. Channel dynamics, sediment transport and the slope of alluvial fans: experimental study. Geology 106, 677–693.

Winterwerp, J.C., Bakker, W.T., Mastbergen, D.R., Van Rossum, H., 1992. Hyperconcentrated sand–water mixture flows over erodible bed. Journal of Hydraulic Engineering, American Society of Civil Engineers 119 (11), 1508–1525.